

Interactions of ${}^6\text{Li}$ and ${}^{133}\text{Cs}$ at Ultralow Temperatures

Peter Scherpelz

March 16, 2009

We study the interactions between lithium and cesium in a magneto-optical trap (MOT) and an optical dipole trap. These collisions are interesting both in terms of their physical properties and due to their ability to either inhibit or aid in the cooling of these two species into degenerate states. In particular, we will study the dependence of the collision properties on the external magnetic field and identify Feshbach resonances between the two species. Here I present the design and testing of the current controller used to drive the magnetic coil and access the Feshbach resonances.

1 Introduction and Background

Interactions between cesium and lithium, which include inelastic collisions, elastic collisions, and the creation of bound molecular states, are interesting for at least four reasons. First, to study lithium and cesium at ultracold temperatures and especially in degeneracy, inelastic collision losses from the trap must be minimized. Second, elastic scattering can influence the performance of sympathetic cooling, which may aid in bringing lithium to degeneracy through its collisions with the typically colder cesium atoms.

Third, bound molecular states may be of fundamental physical interest. One use of ultracold atomic systems is as a model system for more complex quantum phenomena, such as high-temperature superconductivity or quantum chromodynamics. The ability to create and study bound molecular states in this controlled system is therefore extremely important as it opens up a richer set of systems to study. For example, a pairing gap related to superfluidity has been observed using Feshbach resonances with ultracold lithium [1]. Finding different molecular states of lithium and cesium should provide other opportunities for exploring physical theories.

Finally, by loading both lithium and cesium into optical lattices, we hope to perform scalable quantum information processing by using the cesium atoms as messengers between lithium qubits [2]. Realizing this scheme, however, necessitates the implementation of controlled quantum gates, which require a coupling between the lithium and cesium atoms. A weakly bound molecular state could provide this desired coupling.

Weakly bound molecular states are the result of Feshbach resonances, which occur at specific magnetic field strengths [3]. The resonances for cesium and lithium are quite different, with cesium having sharper resonances at smaller magnetic field strengths. Similarly, mixing lithium and cesium may lead to new Feshbach resonances, which would be correlated with currently unknown molecular states. This study necessitates building a controller, presented below, for our magnetic coils. With the controller, we can seek Feshbach resonances over a large range of field strengths.

1.1 Previous Work with Bosonic Lithium

Some of the above phenomena have been explored with ${}^7\text{Li}$ and ${}^{133}\text{Cs}$ [4, 5, 6]. Early experiments used a magneto-optical trap to evaluate the interspecies collision properties. In these studies the excited Li state repelled the ground-state Cs state, so these interactions did not result in trap losses. Ground-state Li, however, can inelastically collide with excited Cs to produce trap losses. If both species are in the ground state, the dynamics present do not result in trap loss until the lithium trap depth is below about 9 GHz, at which point hyperfine collisions are significant [4].

The group went on to study collisions in a dipole trap. They were able to detect the sympathetic cooling of lithium, as well as hyperfine interactions that can result in trap loss [5, 6]. However, we expect many of these interactions to change with ${}^6\text{Li}$. Furthermore, Feshbach resonances are also isotope specific, and were not studied in these experiments.

2 Current Controller Construction

In order to study the interactions across a variety of magnetic fields, one focus of this project is to build an electronic controller for the main magnetic coils in our experiment in order to both access different field strengths easily, and keep the field stable. About 200 Amperes are required from the controller in order to access the broad Feshbach resonance in ${}^6\text{Li}$ around 834 G [3]. We hope to achieve a stability of at least 1 part in 10^4 , and preferably 1 part in 10^5 , when at high currents.

2.1 Controller Design

The current controller requires both a feedback system to stabilize the current output, and the ability to switch the direction of the current through the magnetic coils. To satisfy both of these requirements, we have adopted the design sketched in Figure 1. Current will travel in the same direction through both coils if $I_1 - I_2 > 0$ and $I_3 - I_4 < 0$ or vice-versa. Current direction through only one coil can then be switched by changing the sign of either, but not both, of $I_1 - I_2$ and $I_3 - I_4$.

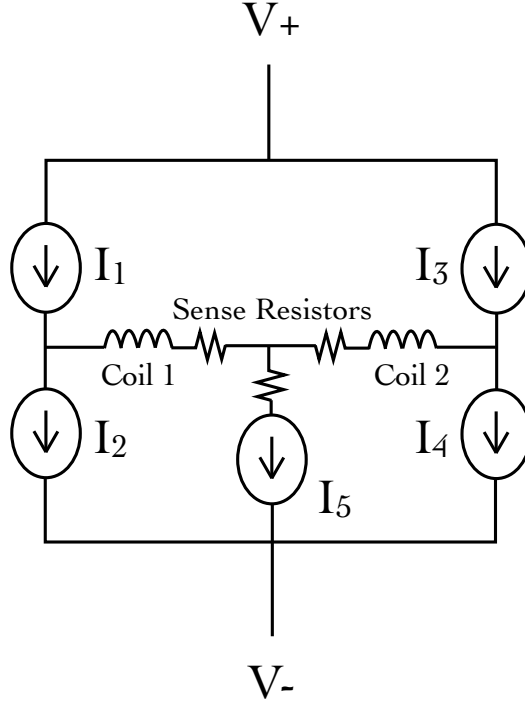


Figure 1: A diagram of the current controller framework. The current sources I_1 through I_4 are controlled by two feedback loops to provide stabilized output to Coils 1 and 2 depending on the current differences $I_1 - I_2$ and $I_3 - I_4$. The three sense resistors are read by the feedback circuits. I_5 is not independent, but is needed to provide the correct voltage drop and current through the center path; it should ideally be less rigid than the other four current sources to provide overall circuit stability. The inductor symbols are taken from <http://en.wikiboks.org/wiki/File:Inductor.svg>.

Sensing the two resistors in series with Coils 1 and 2 provides the input to a feedback loop controlling the sum current traveling through the coils, while sensing the resistor in series with I_5 provides the input to a feedback loop controlling the difference in current between the two coils. The sum current feedback loop outputs two currents, $I_{S1} = I_o + I_s$ and $I_{S2} = I_{o'} - I_s$ where I_o and $I_{o'}$ are bias currents set by potentiometers while I_s is the current set by the feedback. The difference current feedback loop, meanwhile, outputs $I_{D1} = I_{o''} + I_d$ and $I_{D2} = I_{o''} - I_d$, where again $I_{o''}$ and $I_{o'''}$ are bias currents and I_d is set by the feedback loop. We then use current mirrors with a gain G to set

$$\begin{aligned}
 I_1 &= G(I_{S1} + I_{D1}) = I_{1_o} + GI_s + GI_d \\
 I_2 &= G(I_{S2} + I_{D2}) = I_{2_o} - GI_s - GI_d \\
 I_3 &= G(I_{S2} + I_{D1}) = I_{3_o} - GI_s + GI_d \\
 I_4 &= G(I_{S1} + I_{D2}) = I_{4_o} + GI_s - GI_d
 \end{aligned} \tag{1}$$

where I_{1_o} through I_{4_o} are constant bias currents. The gain G here is necessary as I_{S1} , I_{D1} , I_{S2} , and

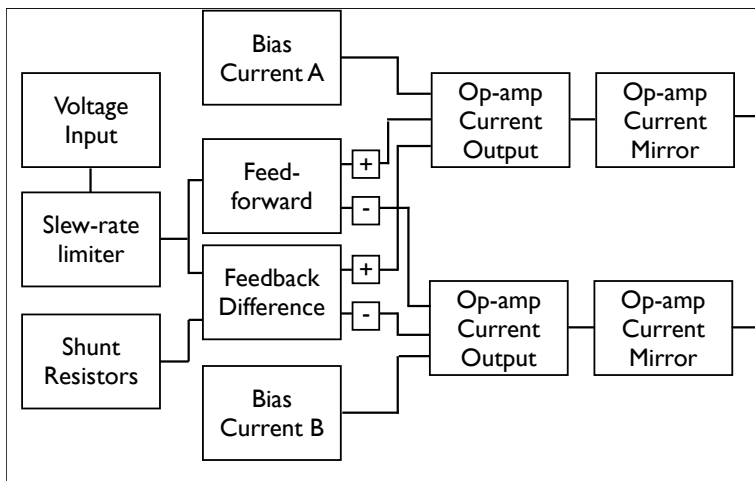


Figure 2: A block diagram of the control circuit. The voltage input is first limited in its slew rate to prevent sudden voltage changes from interfering with the feedback response. This slew rate-limited input is compared to the voltage measured across the shunt resistors to generate the error signal, which is then integrated and sent to the current output as the feedback control. In addition, the input is also delivered directly to the current outputs to improve the speed and allow operation with the feedback loop disabled. Two potentiometers control the constant bias currents. Finally, the current output signal is mirrored with about ten times gain to produce a current output up to about 2 A.

I_{D2} are limited by the feedback circuit design to at most a few Amperes. Thus, to reach 200 A, significant gain must be provided, which is accomplished with a mirror using n-channel field effect transistors, described below.

The average current through both coils, which is equal to $(I_1 - I_2 - I_3 + I_4)/2$, is equal to some constant plus $2GI_s$, so the feedback on the sum current feedback loop will correctly control this average current. The difference in currents, meanwhile, is equal to $I_1 - I_2 + I_3 - I_4$ and is equal to a constant plus $4GI_d$, so the other feedback loop will control only this difference current. Finally, I_5 is set to $I_{5o} + 4GI_d$ to allow the proper current to pass through this channel.

To implement this feedback mechanism, four major components are required. First, the feedback circuits themselves must be constructed and debugged. Second, each output current from the feedback loop must be mirrored into two identical currents. Third, each pair of two currents I_S and I_D above must be summed and then mirrored with gain G . Fourth, the actual current sources must be constructed to handle the high currents required.

2.2 Feedback and Control Circuit

The block diagram of the control circuit is presented in Figure 2, based upon a circuit design by Nate Gemelke. Each current output is determined by a constant bias current, set with a potentiometer, a feedforward voltage input, allowing fast response times, and a feedback input, which is ultimately

responsible for the stability of the system. The feedforward and feedback inputs are sent to the two current outputs with opposite signs, resulting in the proper currents for I_{S1} and I_{S2} , or for I_{D1} and I_{D2} , above.

At this point all parts of this circuit have been tested except for the feedback loop, which will not be tested until the schematic presented in Figure 1 has been implemented. All parts of the circuit functioned properly during testing, except for the current mirror. This was initially implemented with an APEX PA12 power operational amplifier in the inverting configuration displayed in Figure 3.

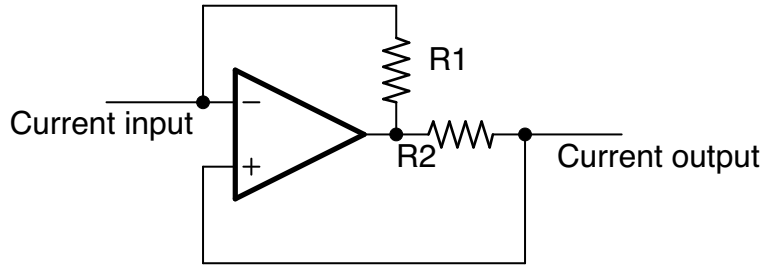


Figure 3: A diagram of the inverting current mirror originally used in the control circuit. The current gain in this circuit is $-R1/R2$. We used $R1 = 10 \Omega$ and $R2 = 1 \Omega$.

However, this configuration created oscillation in both this stage and the previous current output stage of the circuit at about 400 kHz. Adding capacitors to slow down circuit components or varying the output load could bring the oscillation down to below 10 kHz but could not eliminate the oscillation. We then switched to a non-inverting current mirror, displayed in Figure 4, which is stable with similar parameters.

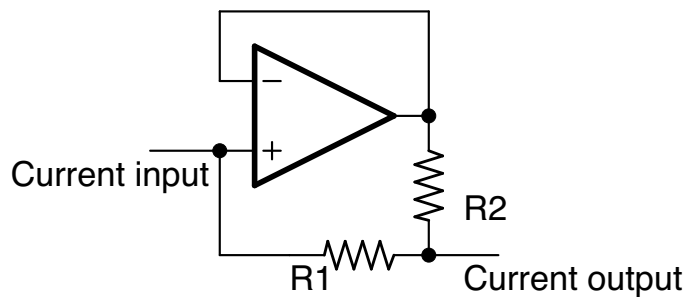


Figure 4: The non-inverting current mirror we are now using in the control circuit. The current gain in this circuit is $1 + R1/R2$. We again used $R1 = 10 \Omega$ and $R2 = 1 \Omega$.

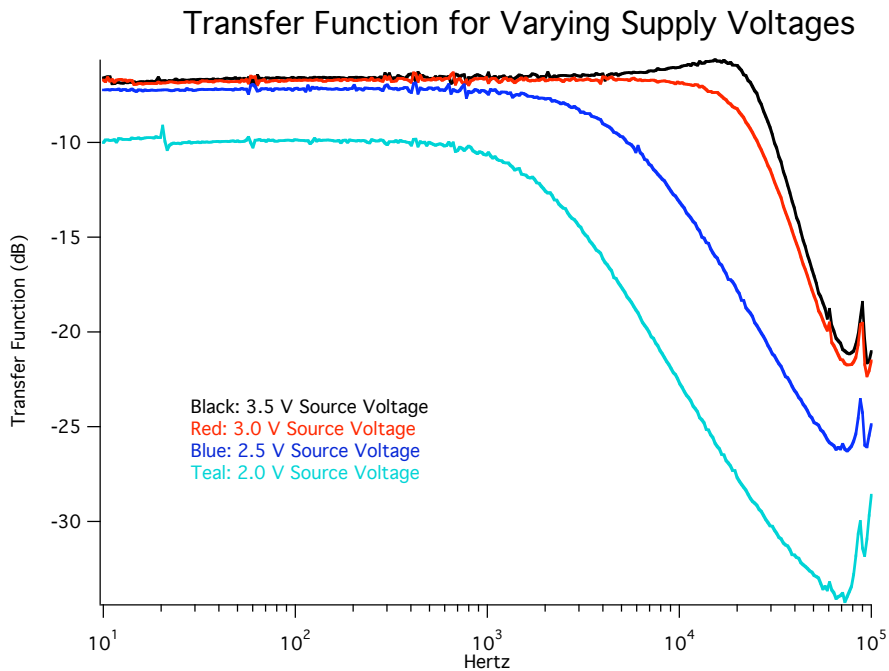


Figure 6: The dependence of the transfer function on the supply voltage, which is the sum of the voltage across the drain and source of the high-current FET and the voltage across the magnetic coil. Here a 15-turn coil with $L \approx 15 \mu\text{H}$ was used. The current across the IRF510 low-current FET was 0.38 A, resulting in about 20 A through the high-current IXFN340N07 FET. In the graph above, as supply voltage decreases, the 3 dB point decreases from 30.4 kHz to 2.2 kHz. The peak in the top curve is probably due to an LC resonance.

from their two drains as well. This design will be tested soon as the control circuit is now functional and the heatsink for the p-channel FETs has also been fabricated.

The second stage of mirroring is done by a pair of two n-channel FETs. We are using an IRF510 n-channel FET for the low-power side that accepts current from the p-channel mirrors. This FET has a similar gain curve to the high-power IXFN340N07 FET, which can supply as much as 100 A of current at DC operation and a voltage across the drain and source of 6 V. These two FETs have similar curves of drain-source current versus the gate-source voltage. As a result, the current input to the IRF510 defines a current across the IXFN340N07 FET which is much larger but approximately linearly related.

This n-channel mirror was tested for stability and speed in isolation from the rest of the circuit. A current output using a PA12 op-amp was provided to the IRF510 FET, and the n-channel mirror was constructed as in Figure 5. A magnetic coil was added in series with the current input to provide inductance and simulate the final setup. The transfer function was then measured with a spectrum analyzer. This system was tested at different temperatures up to 68°C and was stable. It was also tested at total current outputs up to 40 A for one FET and was stable.

Transfer Function for Single FET Versus Parallel FETs

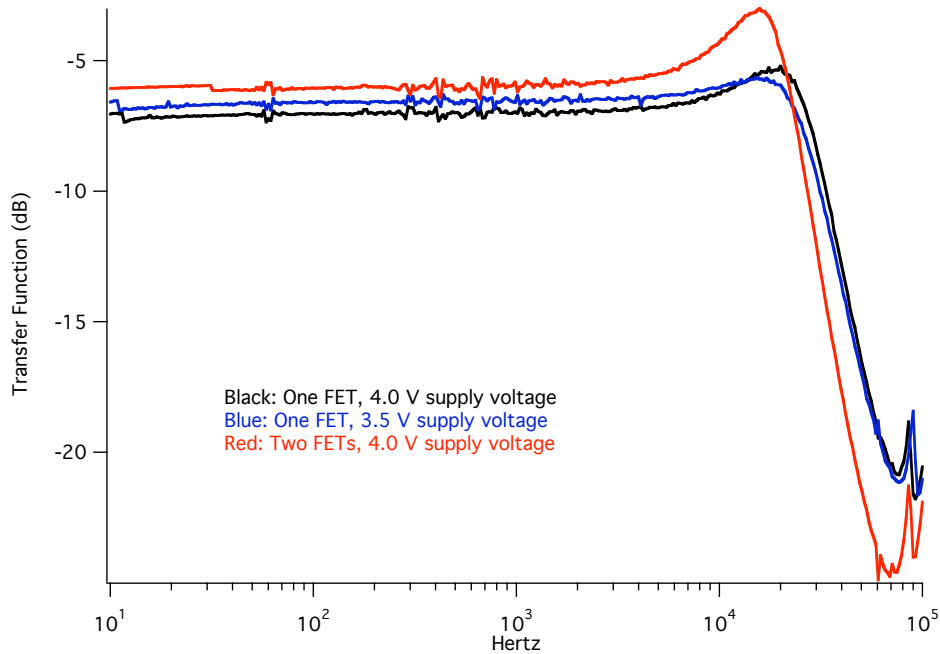


Figure 7: The dependence of the transfer function on the number of FETs. The input current to the IRF510 was 0.38 A in all of these curves. Output current was about 20 A for the single FET and 24 A for the two FETs (demonstrating the two mirrors do not have identical gain, which may be a concern in the future). Both 4.0 V and 3.5 V supply voltages are included for one FET, as the drain-source voltage changes some for two FETs due to the larger total current, and thus larger voltage, through the magnetic coil. The drain-source voltage for the data with two FETs should lie somewhere between the two drain-source voltages for the single FET curves, and overall the 3 dB point for the two FETs is 4 to 6 kHz lower than for a single FET. Also note the higher resonant peak, probably also due to the increased capacitance of the two-FET system.

One critical factor in the speed of the n-channel mirrors is sufficient drain-source voltage for the high-current FET, both due to slew rate and capacitance limitations. The slew rate for current is limited by $dI/dt \leq V/L$ where V is the supply voltage for the high current path and L is the series inductance from the magnetic coil. However, most of the transfer functions should not have been affected by this factor as only the small signal response, and thus very small current changes, were probed. Instead, the capacitance of the FET increases as the voltage across its drain and source decreases, leading to a further slowing of the circuit, which was observed here. Figure 6 shows the effect of decreasing supply voltage in this situation. Note that increasing the inductance of the coil will similarly slow the mirror.

A second critical factor, also relating to the capacitance of the FETs, is the number of FETs in parallel. We hope to use five IXFN340N07 FETs in parallel for each current source I_1 through I_4 , due to the 200 A requirement on their output at a unit duty cycle. Two FETs were tested in

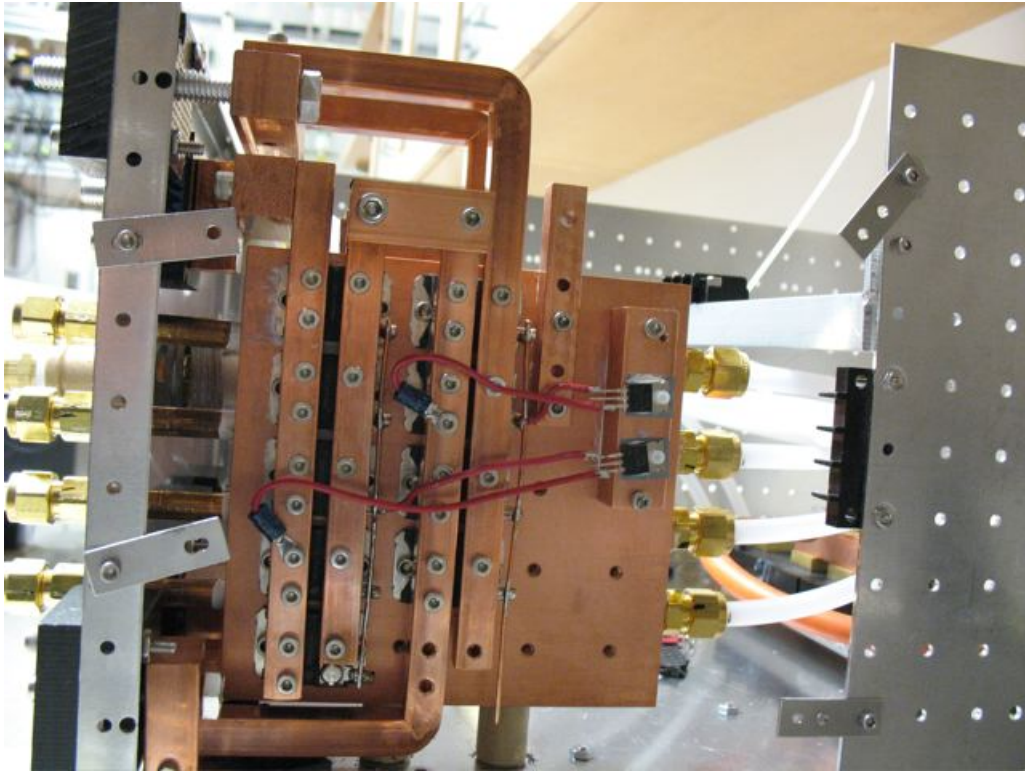


Figure 8: A picture of the heatsink and mounting system. Four water lines run through the heatsink to cool it. Ten FETs (nine shown here) are mounted on each side of the heatsink, as well as the other n-channel mirror FETs on the right.

parallel here. Indeed, the response slowed significantly compared to one FET, as shown in Figure 7.

Overall, the supply voltage will be the critical factor in determining the response. At high currents, the voltage drop across the magnetic coil increases, so the total supply voltage must increase to supply the same voltage drop across the FETs. Similarly, as the number of FETs increases the supply voltage must increase to combat the increased total capacitance of the system. These factors must be weighed against the heatsinking capability of the system, as a voltage increase translates to a proportional increase in power dissipation for the FETs. The FET heatsink has been designed and constructed, and is presented in Figure 8. It is a $6'' \times 6'' \times 1''$ copper block with four $0.375''$ -diameter bores through which chilled water is pumped. This heatsink will be tested in the upcoming weeks to find its maximum power dissipation for safe operating temperatures for the FETs.

3 Conclusion

I have presented the design of a current controller capable of outputting a 200 Ampere current controlled with a feedback loop. The control circuit has been tested and is functional. Furthermore, the n-channel mirror has been tested at up to 40 A in one FET. Typical small-signal responses of the n-channel mirror component are in the 10 kHz range. However, the speed is primarily dependent on the supply voltage and drain-source voltage, which in turn is limited by the heatsinking capability of the system, which has not been tested yet.

References

- [1] Chin, C. *et al.* Observation of the Pairing Gap in a Strongly Interacting Fermi Gas. *Science* **305**, 1128–1130 (2004).
- [2] Brickman Soderberg, K.-A., Gemelke, N. & Chin, C. Ultracold molecules: vehicles to scalable quantum information processing. *ArXiv e-prints* (2008). 0812.1606.
- [3] Chin, C., Grimm, R., Julienne, P. & Tiesinga, E. Feshbach Resonances in Ultracold Gases. *ArXiv e-prints* (2008). 0812.1496.
- [4] Schlöder, U., Engler, H., Schünemann, U., Grimm, R. & Weidemüller, M. Cold inelastic collisions between lithium and cesium in a two-species magneto-optical trap. *The European Physical Journal D-Atomic, Molecular and Optical Physics* **7**, 331–340 (1999).
- [5] Mosk, A. *et al.* Mixture of ultracold lithium and cesium atoms in an optical dipole trap. *Applied Physics B: Lasers and Optics* **73**, 791–799 (2001).
- [6] Mudrich, M. *et al.* Sympathetic Cooling with Two Atomic Species in an Optical Trap. *Physical Review Letters* **88**, 253001 (2002).